Durability Enhancement of Low Ice Adhesion Polymeric Coatings

Halar Memon, Davide S.A. De Focatiis, Kwing-So Choi and Xianghui Hou*

Faculty of Engineering, University of Nottingham, University Park, Nottingham NG7 2RD, UK;

*Correspondence: xianghui.hou@nottingham.ac.uk.

Abstract

Icephobic performance of low-ice adhesion polymeric coatings has been studied intensively for passive ice protection. However, limited efforts were conducted to identify strategies for enhancing the durability of the coatings to maintain low ice adhesion after erosion impact. In this work, we developed and investigated several polyurethane-based nanocomposite and fibre-reinforced coatings to understand the deteriorating behaviour of the coatings under rigorous impinging erosion tests and the subsequent impact on ice adhesion. The inclusion of fillers resulted in up to 38 points increase in Shore hardness relative to the pristine PU coatings. The ice adhesion strengths on 3 wt% nanoparticle-reinforced coatings after the erosion tests were nearly halved, whereas, a 5-fold reduction was observed on 3 wt% fibre-reinforced coatings compared to that of the pure PU coatings. Our results indicated that the incorporation of fillers was effective in reducing the ice anchoring points, and that, after the impingement, the icephobic performance was retained by either lowering surface roughness or by minimizing surface deterioration. Fibres took a more effective role in limiting crack initiation and resisting crack propagation. The ice adhesion strength of the coatings increased from 5.6 kPa to 8.4 kPa with 20 wt% carbon fibres incorporated PU coatings, essentially keeping the adhesion below 10 kPa even after rigorous impinging tests and a ~10-fold reduction in ice adhesion strength as compared to the pure PU coatings. The incorporation of the fibres led to enhanced durability and retention of excellent icephobic performance via a mechanism that is adaptable to other polymeric coatings.

Keywords: Carbon fibres, ice anchoring, durability, icephobicity, polyurethane

1 Introduction

Polymeric surfaces and coatings have been a popular choice for passive ice protection and many reports have indicated low ice adhesion strength on polymeric coatings and surfaces [1-4]. Polydimethylsiloxane (PDMS) and polyurethane (PU) are the major candidates in the development of icephobic coatings, and their icephobic performance has been studied intensively [5-7]. However, limited efforts have been paid on the durability of the coatings and their capability to maintain icephobic performance after erosion impact. Most studies have either conducted icing/de-icing cycles [8-11], chemical stability [12-14], and/or durability evaluation using mechanical methods (such as abrasion resistance, indentations, scratch tests, and sandblasting etc.) [14-18]. Wu et al. [19] tested their sol-gel coatings by nanoindentation, pencil-scratch resistance, and weight loss rate under different sandblasting conditions, indicating that the measured ice adhesion strength was maintained below 70 kPa after mechanically endured durability tests. Beemar et al. [20] reported an ice adhesion strength at around 6 kPa, even after 1000 abrasion cycles on a PDMS gel surface. Zhuo et al. [21] measured an increase in ice adhesion strength from 12 kPa to 20 kPa after 800 abrasion cycles on a PDMS coating. Liu et al. [22] carried out an impinging study on a PDMS nanocomposite coating using a silicon carbide suspension at 37 m/s velocity and a liquid flow rate of 72 mL/min, but did not re-evaluate the ice adhesion strength after the impinging erosion.

The research interest to explore the inclusion of hard materials in a soft polymer matrix is overwhelming, and many studies have been conducted to investigate the mechanical properties of composites reinforced with fibrous and/or nano inclusions [14-18]. The key application areas of icephobic coatings are in aerospace and wind energy, both of which involve rigorous water droplet erosion. A leading edge of aircraft often suffers ice crystals impingement in sub-zero temperatures and/or rain droplets erosion. Wind turbine blades may undergo severe water droplet impingement as well and coating erosion resistance under the working conditions is also critical. Therefore, the designed icephobic coatings need to resist such surface erosion damage (morphological and/or topographical) that may deteriorate the icephobic performance.

In this study, polyurethane (PU) based low ice adhesion coatings were formulated and reinforced with nanoparticles and micro-fibres. The main aim of this study was to explore an effective approach to enhance the durability of the icephobic coatings. The incorporation of micro-fibres and nanoparticles in this work was driven by the need to enhance durability in surface icephobicity under erosion impact, even after non-ignorable material damage. Water impinging tests using silicon carbide (SiC) particle suspension were used to simulate the water droplet erosion. It was suggested that the inclusion of fibres was more beneficial in this context than the nanoparticles. The addition of fibres helps to distribute the droplet impact energy more widely across the polyurethane matrix and helps to reduce the stress concentration points on the coating surface by minimizing crack initiation during the incubation period. Thus, less ice anchoring on the surface would be formed, leading to easier ice removal and maintaining the desirable icephobic performance even after the erosion impacts.

2 Experiments

Four types of polyurethane coatings were formulated in this study, and each coating was characterised and compared in terms of surface roughness, morphology, and ice adhesion strength before and after the impingement test.

2.1 Substrates and raw materials

Aluminium 2024-T4 plates with a size of 50 mm x 20 mm x 1 mm were used as substrates. A two-part thermoset polyurethane resin, PMC-790 (PU), was purchased from Smooth-on

(USA). Kevlar Aramid pulp, Twaron ® 5011 (Kevlar fibres, 125 µm average length), was kindly provided by Teijin Aramid GmBH (Germany). Carbiso Mil 100µ (milled carbon fibres, 80-100 µm average length) was obtained from easycomposites (UK). Reduced graphene nanoplatelets, CamGraph G3 (GR, lateral size of ~400 nm and flake thickness of ~3 nm), were purchased from FGV Cambridge Nanosystems (UK). Nanodiamonds powder (ND, spherical size ≤100 nm) was procured from Jichang Metal processing Ltd. (China). Silicon carbide particles (SC224 600 mesh) for the water impinging erosion test were supplied by Simba Materials (UK). Triton X-100 was purchased from Sigma-Aldrich (UK). All materials were used as received.

2.2 Preparation of coatings

All aluminium plates were sandblasted to enhance the coating adhesion, using a Guyson F1200 sandblaster with 180-220 µm alumina particles. The substrates were then washed with ethanol and deionized water thrice and dried using compressed air before the coating application.

PU solutions were magnetically stirred at a Part A : Part B ratio of 2 : 1 by weight as listed in table 1. Different fillers were introduced and mixed in the resin solution during the stirring, The PU resins were then ultrasonically mixed for a further 30 minutes, and brush coated on the sandblasted aluminium substrates. All PU coatings with and without fillers were cured at 25 °C for 48 hours and post-treated at 65 °C for 4 hours.

Table 1: List of sample types and their compositions

Sample types	**Sample codes**	**Coating type**	**Filler content (wt%)**
Pure PU coatings (PU)	PU	Pristine	-
PU coatings with carbon fibres (PU-CF)	PU-CF-0.5	Fibre-reinforced	0.5
	PU-CF-1		1

	PU-CF-3		3
	PU-CF-5		5
	PU-CF-20		20
PU coatings with Kevlar fibres (PU-KV)	PU-KV-0.5	Fibre-reinforced	0.5
	PU-KV-1		1
	PU-KV-3		3
	PU-KV-5		5
	PU-KV-20		20
PU coatings with nanodiamond (PU-ND)	PU-ND-0.5	Nanocomposite	0.5
	PU-ND-1		1
	PU-ND-3		3
	PU-ND-5		5
	PU-ND-20		20
	PU-ND-40		40
PU coatings with graphene (PU-GR)	PU-GR-0.5	Nanocomposite	0.5
	PU-GR-1		1
	PU-GR-3		3
	PU-GR-5		5

2.3 Surface characterization

A Zeta-20 non-contact optical profiler was used to evaluate the surface roughness. The roughness values reported were the average of a minimum of 30 measurements, and R_a was measured over a line stretching across the observed surface. The same system was used to observe topographical changes on the surfaces after erosion. An FEI Quanta 650 ESEM (environmental scanning electron microscope) was used to acquire microstructural images and morphological changes on the eroded coatings.

Shore hardness was measured using a SAUTER durometer having Shore hardness A and D scales. The durometer was attached to SAUTER test stands TI-AO and TI-D for Shore hardness A and D scales, respectively. The hardness reported was an average penetration (Shore) value based on 10 separate measurement. Supplementary table 1 outlines the complete data of surface roughness and Shore hardness measurements.

2.4 Evaluation of hydrophobicity and icephobicity

The sessile drop technique was used to measure water contact angles (WCAs) using an FTÅ200 goniometer and 5 µl water drops were used. The tests were conducted at room temperature, and further details of the measurement were described in our previous work [23, 24].

A MOOG G403-2053A servo motor was used to measure the ice adhesion strength tests via a centrifugal method and the test was performed in an environmental chamber (ALPHA 1550-40H) to simulate the freezing conditions. The ice adhesion test was conducted at a temperature of -10 °C and the testing method was described previously [23, 24]. The ice formation and ice adhesion test were conducted at -10 °C and are depicted in figure 1. The bulk ice formation was carried out using a silicon mould attached on the coating surface, as shown in figure 1a. The samples were then spun in the centrifugal chamber with a counterweight (figure 1b) and the speed at the time of ice detachment was obtained.

The centrifugal shearing force F (N) is determined from Eq. (1):

$$F = mr\omega^2 \tag{1}$$

where ω (rad/s) is the rotational speed at the point of ice removal, r (m) is the rotor length, and m (kg) is the mass of ice. The ice (shear) adhesion strength τ_{ice} can then be calculated as

$$\tau_{\text{ice}} = {}^{F}\!/_{A} \tag{2}$$

where A (m^2) is the substrate/ice contact area.

The centrifugal method to evaluate the ice adhesion strength in this work had been previously applied by many researchers [25-27] and a recent comparative study indicated its compatibility with the other widely used methods such as horizontal force transducer method [28]. However on bulk ice formations, the study indicated a systematically higher shear strength on the push methods as compared to that of the centrifugal methods. The static and dynamic water contact angles (WCAs), including advancing WCAs (AWCAs), receding WCAs (RWCAs), contact angle hysteresis (CAH), and ice adhesion strength measurement are summarized in supplementary table 1.

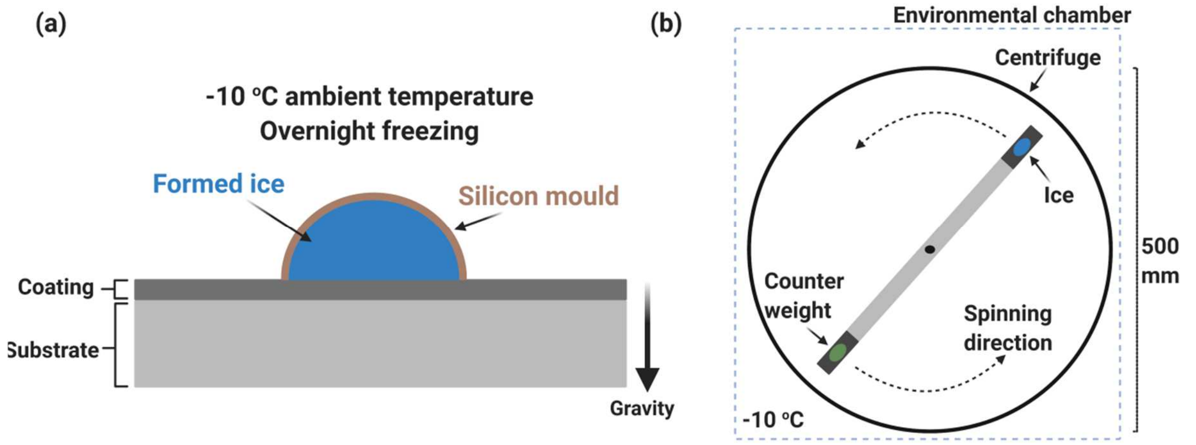

Figure 1: (a) Ice formation on a sample surface and (b) the details of the centrifugal testing method (figure created using biorender.com)

2.5 Water impinging erosion tests (WIETs)

To evaluate the coating durability, erosion tests from the impingement of silicon carbide aqueous suspension were carried out. The silicon carbide suspension was prepared using 1 wt% silicon carbide microparticles and 0.1 wt% of Triton X-100. The suspension was then magnetically stirred for 4 hours. During the impinging test, the suspension was pressurized through a PNR ultrasonic atomiser nozzle (MAD 0331 B1BB) using compressed gas and the micro-droplets impinged onto the coating specimen. The system was maintained at a liquid flow rate of 1.2 mL/s, a distance between the nozzle and the specimen of 4 cm, and a duration of 90 minutes. The method had been described in detail elsewhere [22]. The surface morphology, surface roughness and ice adhesion strength of the coatings were measured before and after the erosion tests.

3 Results and discussion

3.1 Effect of incorporated fillers on coating hardness

The pure PU coatings exhibited a Shore hardness of 40D, and the incorporation of fillers increased the hardness, especially for PU-KV-5, where 24 points increase was observed to 64D. The incorporation of fillers in PU-GR and PU-CF coatings led to an enhancement of the hardness. However, the increase in hardness was relatively insensitive to the amount of filler as shown in figure 2. In the PU-KV and PU-ND coatings, a significant increase in the hardness was observed with increasing filler content. Generally, the inclusion of fillers increased the hardness of the polymeric coatings by 12~62%. Shore hardness values could be used as representative values for elastic modulus [29] and the representative values are equivalent to elastic modulus measured via other typical methods [30].

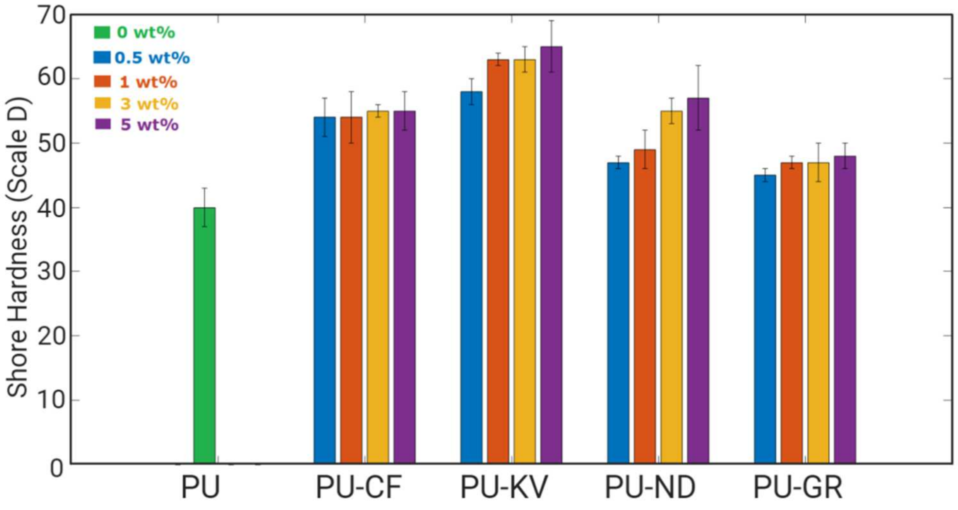

Figure 2: Effect of fillers on the Shore D hardness of polymer coatings

3.2 Microstructural observation of the polymeric coatings

The influential role of surface roughness on ice adhesion strength is mainly due to the ice anchoring process on the surface [23, 24]. As the material suffers erosion attack, the surface morphology is randomly deteriorated in a way that could influence the icephobic performance of the coatings. The impinged surface may generate some ice anchoring points which would increase ice adhesion strength due to mechanical interlocking of the ice on the surface. Changes in the surface roughness on all the coatings as a result of the impingement were also measured and listed in supplementary table 1.

3.2.1 PU coatings

The microstructural images of the pristine PU coatings and their surface after WIETs are shown in figure 3. It is evident that the surface morphology had been significantly altered and the surface was much rougher after WIETs. The impinging water droplets and SiC particles created cavities on the surface as shown in figure 3b. The surface roughness (R_a) also drastically increased from 0.08 µm to 0.45 µm on the PU coatings after WIETs. The pure PU coating was also studied over a larger area and the 3D profile of an impinged PU coating is shown in supplementary figure 1a. The figure shows a valley where the cavities are ~25-80 µm deep, making them easy to induce mechanical interlocking of ice. The initial water condensation and subsequent ice formation had been observed in the surface cavities in our previous work [23, 24].

3.2.1.1 Polymeric nanocomposite coatings

The surface morphology of PU-ND-3 coatings (figure 3c), has also changed considerably after WIETs. The surface morphology of PU-GR-3 compared with PU-ND-3 coatings after WIETs are provided in supplementary figure 2a and 2b. The PU-GR-3 and PU-ND-3 coatings had surface roughnesses (R_a) of 0.1 µm and 0.07 µm respectively before WIETs, and a clear increase in surface roughness to 0.21 µm was observed on both nanocomposite coatings after WIETs. Notably, the change in surface roughness was much lower than that observed on the pure PU coatings, indicating that the incorporation of fillers resisted the erosion attack on the nanocomposite surfaces. A mixture of cracks and cavities were formed after WIETs on the surface of PU-ND-3 coating (figure 3c), instead of the cavities observed on the pure PU coatings in figure 3b. 3D surface profiles of PU-ND-3 and PU-GR-3 are given in supplementary figure 1b and 1c, respectively. The depth of cavities is considerably reduced on both nanocomposite coatings as compared to the pure PU coatings, and the cavities are up to 25 μm deep.

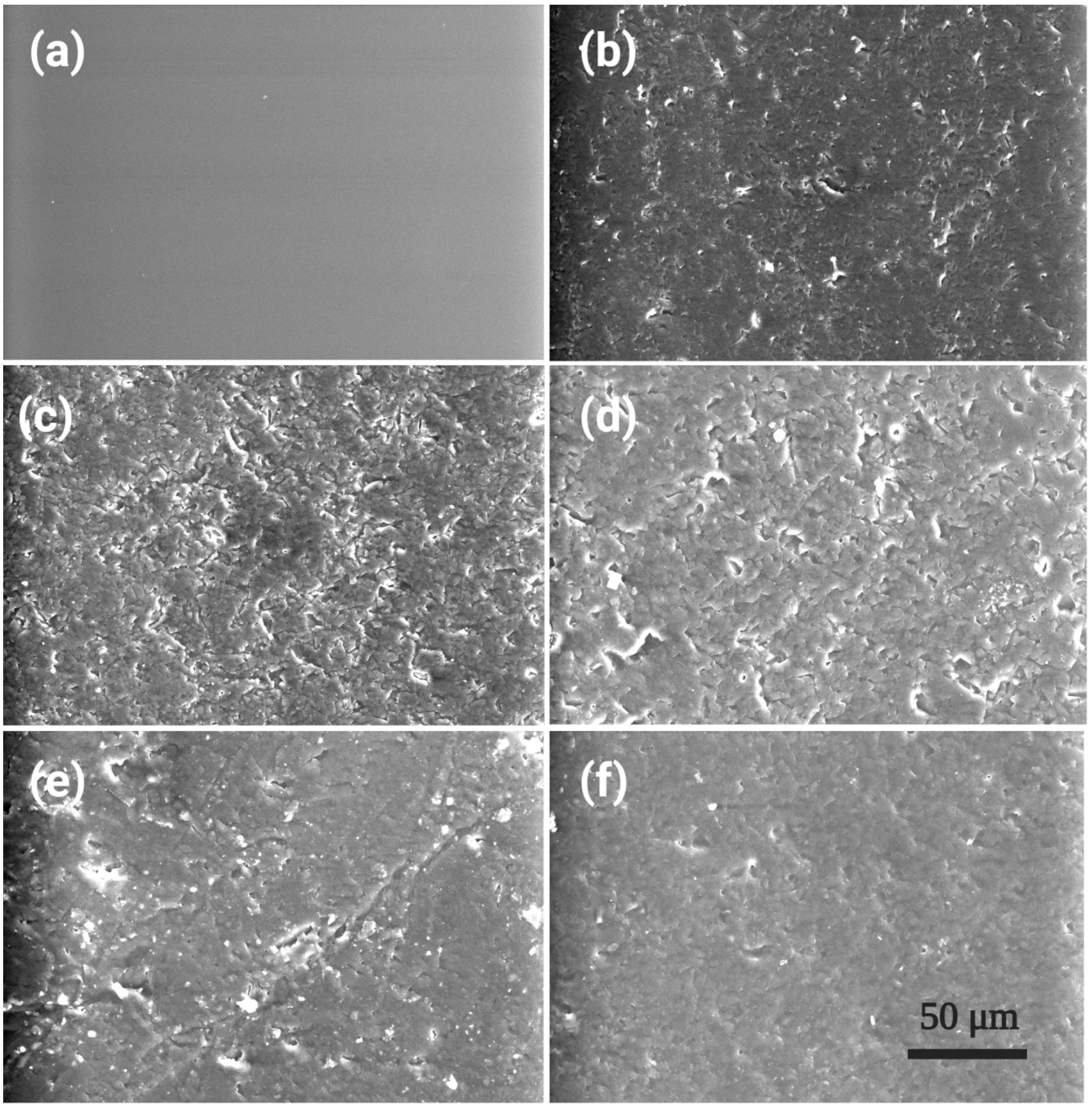

Figure 3: Microstructural images of (a) before and (b) after WIETs on the pure PU coatings and after WIETs on (c) PU-ND-3, (b) PU-ND-20, (e) PU-KV-3, and (f) PU-KV-20 coatings

3.2.1.2 Polymeric fibre-reinforced coatings

The microstructural image of PU-KV-3 coatings after WIETs is shown in figure 3e. Similar images after WIETs on PU-CF-3 compared with PU-KV-3 coatings are given in supplementary figure 2c and 2d, respectively. Surface roughness (R_a) changed from 0.07 μm on PU-CF-3 coatings to 0.27 µm and from 0.10 µm on PU-KV-3 coatings to 0.25 µm after WIETs. Both impinged fibre-reinforced coatings indicated a larger increase in surface roughness as compared to the impinged nanocomposite coatings. Closer inspection of figure 3e and supplementary figure 2c suggests that a significant portion of polymeric surface was largely intact and the fibres were effective to restrain crack initiation, significantly reducing the number of surface cavities.

The material damage around the fibres in the composite coatings is shown in figure 5c and 5d. 3D profile of impinged PU-KV-3 surface, shown in supplementary figure 1d, indicates the surface damage incurred after the erosion tests. The 3D profile of impinged PU-CF-3 coatings is shown in supplementary figure 1e. The cavities on both fibrous coatings are ~40-70 µm in depth.

3.2.2 Inclusion of high weight percentages of fillers

In section 3.2.1, the coatings incorporated with 3 wt% fibres demonstrated more promising results in terms of maintaining icephobic performance than the equivalent loading of nanoparticles. In this section, coatings with higher filler contents were prepared to explore the possibility of enhancing the durability of the polyurethane matrix. This could further reduce the number of ice anchoring points and help to maintain low ice adhesion strength.

3.2.2.1 PU nanocomposite coatings

The incorporation of nanodiamonds in PU coatings was limited to a maximum of 40 wt%. Further incorporation was difficult to process as the formulated solutions were highly viscous, thus, not suitable for the brush application. The surface roughness (R_a) changed from 0.21 µm to 0.24 ± 0.03 µm (slight increase) on PU-ND-20 and from 0.21 µm to 0.17 ± 0.02 µm (slight decrease) on PU-ND-40 before and after WIETs. Overall, the surface roughness after WIETs decreased with a higher concentration of nanodiamonds. The surface morphology of PU-ND-40 coating after WIETs and the surface cavities generated are shown in figure 4a and 4b, and the cavities have the depth around 13 μm, whereas those on PU-ND-3 surface are ~25 μm deep (supplementary figure 1b).

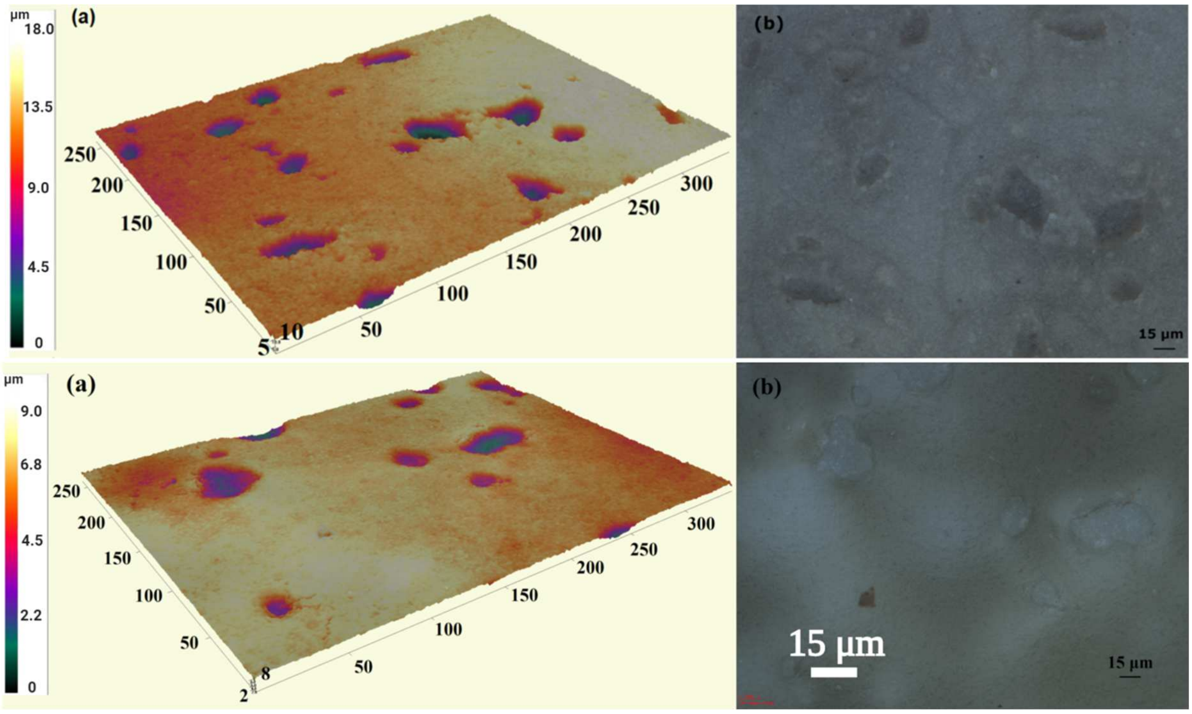

Figure 4: (a) 3D profile and (b) 2D image of PU-ND-40 coatings and (c) 3D profile and (d) 2D image of PU-KV-20 coatings after WIETs

The morphological changes on PU-ND-3 and PU-ND-20 surfaces are shown in figure 3c and 3d, respectively. It is clear that the morphological damage on the surface was further reduced with a higher concentration of nanodiamonds and the number of cavities was considerably reduced. Figure 3d indicates that the cavities on PU-ND-20 surface, which could be ice anchoring sites, were reduced in both the numbers and the depth when compared to those on PU-ND-3 coatings, as shown in figure 3c.

3.2.2.2 Fibrous PU coatings

A maximum of 20 wt% of Kevlar and carbon fibres were incorporated in the PU matrix, and the microstructural images of both fibre-reinforced coatings after the erosion damage are shown in figure 4b and supplementary figure 3. Both coatings demonstrated promising durability during WIETs and the surface roughness did not change significantly compared to that on as-prepared surfaces. The surface roughness (R_a) on PU-CF-20 coatings changed from 0.12 μm to 0.15 μm after WIETs, and from 0.12 μm to 0.22 μm on PU-KV-20 coatings. The 20 wt% fibre-reinforced coatings demonstrated the lowest increase in surface roughness after WIETs across all the studied coatings. The depth of cavities on PU-KV-20 coatings was in the range of ~2-7 μm, nearly halved in magnitude compared to those on PU-ND-40 coatings.

The number of cavities was also reduced on the 20 wt% fibre-reinforced coatings as compared to those on the 3 wt% fibre-reinforced coatings. A comparison between PU-KV-3 and PU-KV-20 coatings is shown in figure 3e and 3f. The high filling of fibres in polyurethane coatings was in favour of resisting the microstructural damage caused by the erosion. Less number of surface cavities was observed on the 20 wt% fibre-reinforced coatings, and the depth of the cavities was also reduced. In terms of fibres, carbon fibres in this study were more effective in resisting the morphological changes when compared to Kevlar fibres, as shown in figure 5a and 5b. Figure 5 also indicates an obvious size reduction of the cavities on PU-CF-20 coatings and the size of cavities is significantly reduced (around 10 μm).

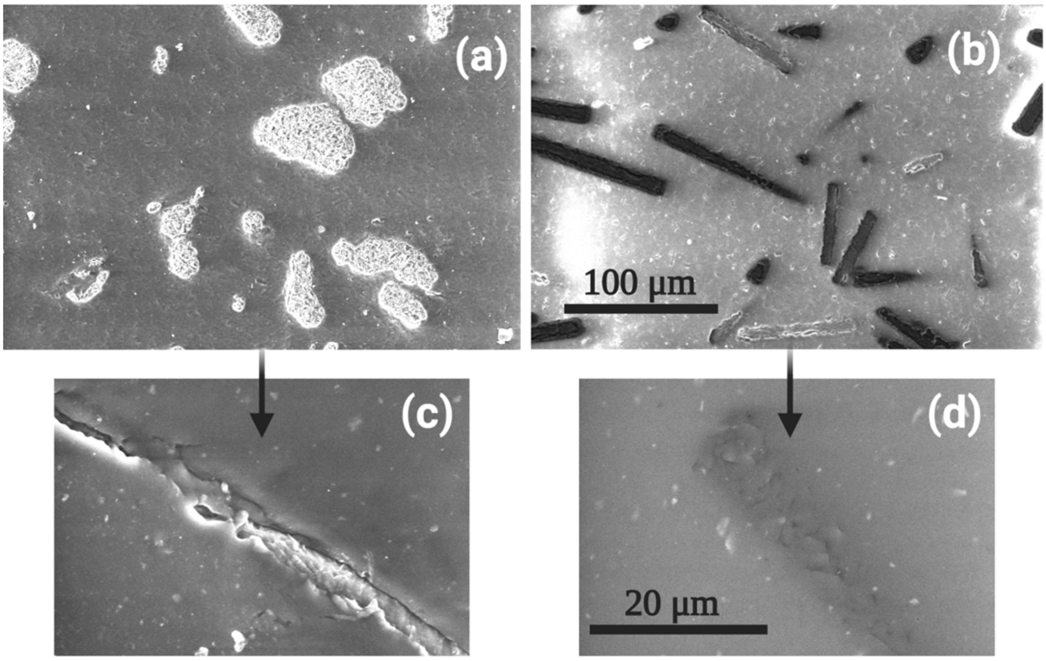

Figure 5: (a) PU-KV-20 and (b) PU-CF-20 coatings after WIETs. Possible material damage around the incorporated (c) Kevlar and (d) carbon fibres

3.2.3 Impact of impinging erosion on ice adhesion strength

Many researchers have used cyclic de-icing tests to evaluate icephobic performance of the coatings [8-11] and abrasion tests to evaluate the durability icephobic coatings [14-18]. However, the impingement test is more representative of real-application conditions to evaluate the coating durability when considering the potential applications in aerospace and wind turbine. Ice adhesion strengths, before and after WIETs, on specific coatings are shown in figure 6d. Generally, the coating hardness had a direct effect on ice adhesion strength.

3.2.3.1 Pre-impingement tests

Ice adhesion strengths on all the as-prepared samples were less than 7 KPa, except for PU-KV-0.5, PU-KV-20, and PU-GR-5 coatings, as indicated in figure 6b. Higher ice adhesion strengths on PU-KV-20 and PU-GR-5 are thought to be due to the changes in morphology resulted from the higher filler concentrations. PU-KV-0.5 is an exception and its relatively high ice adhesion strength may be mainly attributed to surface defects formed during the coating preparation, which is evidenced by the higher surface roughness as listed in supplementary table 1. A direct relation of ice adhesion strength with shore hardness is drawn in figure 6a. For example, the incorporation of 20 wt% of Kevlar fibres in the PU matrix leads to an increase in shore hardness to 78D and a 4-fold in ice adhesion strength was measured. The incorporation of fillers could alter the surface characteristics and influence the ice formation process, as observed in the PU-KV-0.5 coatings. Generally, the ice adhesion strength increased with the incorporation of fillers, but they were mostly kept under 10 kPa before WIETs.

3.2.3.2 Post-impingement tests

The ice adhesion of the pristine and impinged PU coatings is 2.6 kPa and 83.1 kPa respectively, indicating approximately 32-fold increase after the erosion. Compared to the values of the pure PU coatings, the ice adhesion strength of PU-GR-3 coatings after WIETs was nearly halved. Similar results were also observed on PU-ND-3 coatings for which the ice adhesion strength changed from 2.7 kPa to 45.4 kPa after WIETs. This value of PU-KV-3 coatings changed from 5.1 kPa to 16.1 kPa after WIETs; while on PU-CF-3, it increased from 5.6 kPa to 16.8 kPa. Overall, the ice adhesion increased by approximate 3 folds on the 3wt% fibrous PU coatings after WIETs. The incorporation of high filling of nanodiamonds (higher than 3 wt%) resulted in reduced ice adhesion as compared to that of PU-ND-3 coatings. The ice adhesion strength on PU-ND-20 coatings decreased from 39.9 kPa to 28.9 kPa on PU-ND-40 coatings. The increase in ice adhesion on PU-KV-20 and PU-CF-20 coatings after WIETs was 1.4 fold and 2-fold, respectively. Compared to the pure PU coatings, a ~10-fold reduction in ice adhesion strength after WIETs was obtained on the PU-CF-20 coatings, whereas it was a ~5-fold reduction on the PU-KV-20 coatings.

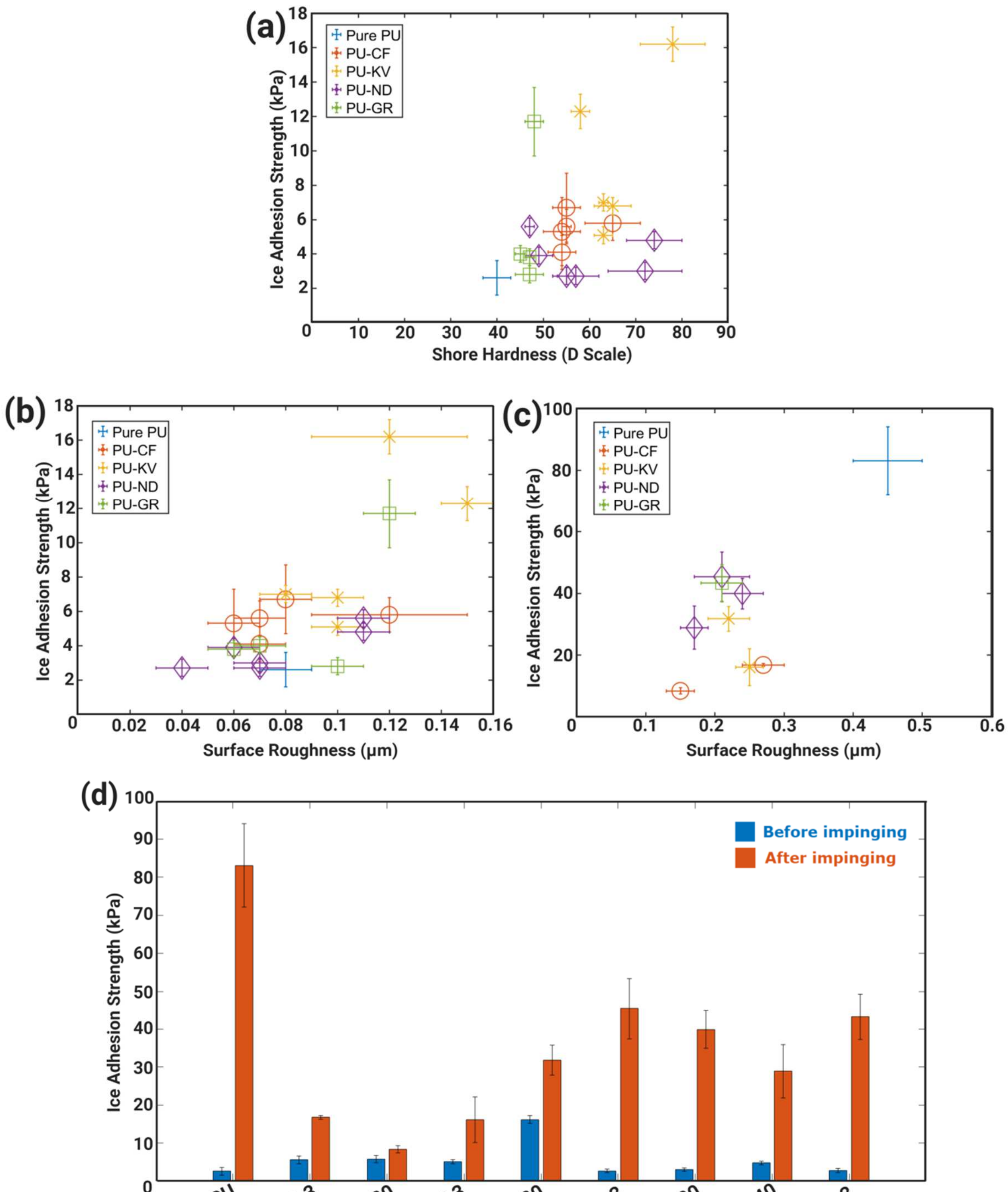

Figure 6: Ice adhesion strength in comparison to (a) Shore D hardness values, surface roughness (b) before and (c) after WIETs. (d) Ice adhesion strength before and after WIETs

The incorporation of fillers was effective in resisting the formation of larger and/or deeper cavities, as shown in figure 3, and the possible ice anchoring was either reduced or weakened. These specific changes in ice adhesion strength indicate that the post-impingement icephobic performance was intrinsically dependent on the filler contents and structures. Fibres are likely to induce less ice anchoring points and fewer microstructural changes after WIETs. The ability of ice to anchor on the surface is highly reliant on the surface roughness [23, 24], and the post-impingement ice adhesion is plotted against the impinged surface roughness in figure 6c. It is evident that the fibre-reinforced surfaces minimized the surface crack propagation and there were fewer anchoring points available, thus facilitating the removal of ice. The figure also highlights the dominating role of surface roughness and no apparent correlation with the relation to shore hardness values is observed. Fundamentally, the inclusion of fillers results in improved durability of the PU coatings. In terms of icephobic performance, it is impressive that PU-CF-20 coatings still maintains the ice adhesion strength below 10 kPa after the silicon carbide suspension impinging erosion, and only a 1.4 fold increase in ice adhesion strength is observed, which is a significant improvement as compared to that on the pure PU coatings.

3.3 Surface durability enhancement mechanisms

The enhanced durability on the polymeric coatings could be explained in two distant mechanisms: surface characteristics and erosion resistance. Firstly, polymeric coatings with low elastic modulus are likely to induce low ice adhesion strength. It was reported that ice adhesion strength decreased with the decrease of polymeric cross-link density [13, 31]. From literature, the incorporation of Kevlar fibres, carbon fibres, nanodiamonds [32-34], and graphene [35] often indicated a significant increase in mechanical properties of the polymeric matrix. The Shore hardness measured in this work also indicts the enhanced hardness after the incorporation of fillers, which also suggests an increase in the elastic modulus [29]. Thus, the results support the need to lower down elastic modulus of polymers to induce a low ice adhesion. However, ice shear mechanism is a complex phenomenon and requires similar surface characteristics to draw conclusions. The surface roughness of the coatings is a dominating factor for the ice adhesion strength [24]. Surface anomalies or cavities play an important role and could encourage ice anchoring that may enhance ice adhesion strength. The incorporation of carbon and Kevlar fibres produced mechanically reinforced composite coatings. However, at 20 wt% fibres loading, the Kevlar-reinforced coatings suffered higher damage, evidenced by the deeper and wider cavities as compared to those on carbon fibres reinforced coatings. The damage on PU-KV-20 coatings could be explained from the fibre interface bonding and the fibre aspect ratio. Firstly, In terms of fibre interfacial bonding with the polymeric matrix, carbon fibres demonstrated higher interfacial strength than Kevlar fibres, as reflected from the eroded coating surface: the carbon fibre was still tightly packed in the polyurethane matrix, whereas the Kevlar fibre was exposed after the erosion impact (figure 5c and 5d). Secondly, the interfacial bonding of fibres is closely related to the toughening mechanisms, such as fracture energy and fracture toughness, and the work of fracture would be greatly increased due to interfacial friction between the matrix and fibres [36]. Lastly, the mechanical properties were demonstrated to be strongly dependent on the aspect ratio of the reinforcing fibres, and the aspect ratio of the carbon fibres (~14) used in this work is much higher than that of Kevlar fibres (~3). It is believed that filler with a higher aspect ratio would provide greater resistance against erosion impact [37].

Secondly, the erosion of material induces cracks on the surface. The crack initiation and propagation can be described as a combination of four mechanisms: (1) direct removal of material or deformation caused by the direct high-speed impact; (2) propagation of stress waves across the material; (3) fatigue incurred by the surface with repetitive droplet impinging; (4) the inability of material to elastically recover (progression into plastic deformation region) before the next impact event [38]. The erosion resistance depends on how the material behaves at the impact zone and how stress waves generated at the impact zone are propagated to the rest of the solid target. These stress waves consist of three multidirectional waves as illustrated in figure 7a [39]. The velocities at which these waves propagate depend on the material density, Poisson's ratio and elastic modulus of the target. Microstructural discontinuities also result in enhanced stress waves due to stress concentrations on the surface, and the material may experience structural failure if the stress waves exceed the dynamic fracture strength of the target material [40].

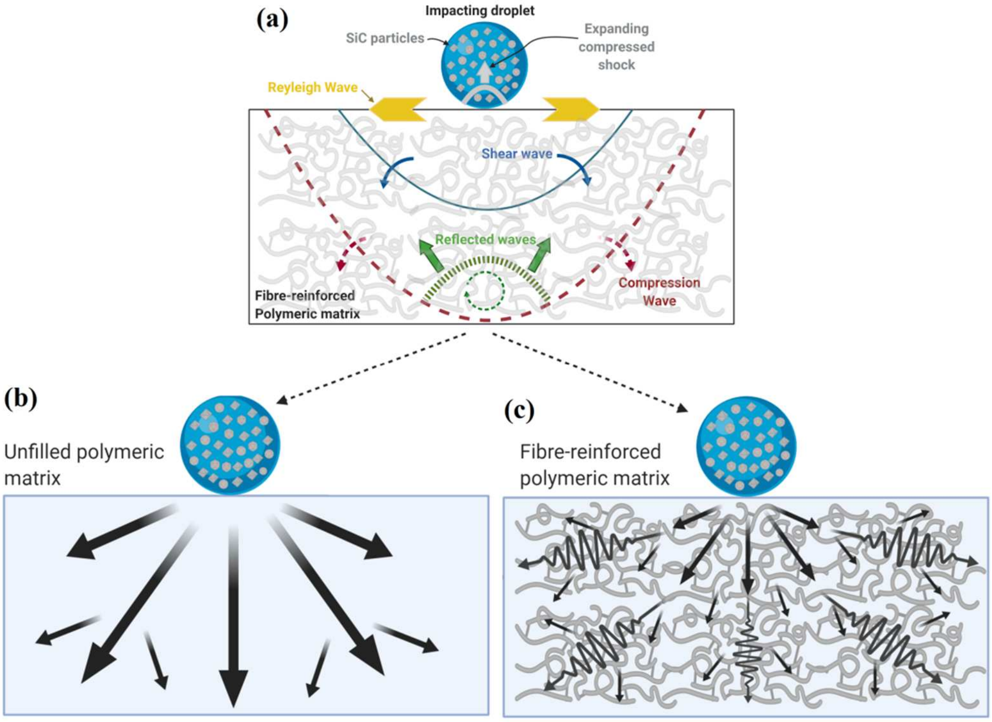

Figure 7: (a) Stress waves generated after the impact of a water droplet/sand particles (The mechanism is adapted from [39]) and the stress waves on (b) a pristine polymer and (c) a fibre-reinforced polymer (figure created using biorender.com)

Erosion resistance of the polyurethane coatings, thus, could be imparted by carefully selecting and incorporating fillers in the matrix in order to distribute the stress waves effectively. However, it is imperative to understand the causes that initiate the erosion deterioration in the coatings and which material properties could be linked to erosion initiation. Erosion initiation in wind turbine blades has been widely debated and surface fatigue was identified as a key failure mechanism [41-43]. Fatigue of the coating during erosion can be explained using two mechanisms. Firstly, water impinging is a form of repetitive loading and the fractures are often observed after the spot has been struck by several impacts [44]. In this work, the impingement test consists of a mixture of water with hard SiC particles, and the particles could inflict a higher scratch and cause more damage upon impact as compared to water droplets, as illustrated in figure 7b. The depletion and deterioration of the surfaces caused by impinging particles were also observed in figure 3, 4, and 5. Secondly, the fractures caused by the erosion may lead to a fatigue failure [45]. However, Alder et al. [46] indicated that fatigue may play a secondary role. They found that the topological changes in the surface or cracks initiations during the incubation period are the main factors that accelerate the erosion rate. Thus, erosion resistance could be imparted in the polymeric coatings by deploying materials and/or incorporation of fillers that limits crack initiation and propagation, and preventing the generation of stress concentration points which may accelerates the erosion rate [47]. These cracks may also prompt the possible formation of ice anchoring points, resulting in the mechanical interlocking of ice on the surface. Thus, preventing the crack initiations on the surfaces has clear advantages for maintaining icephobic performance.

High erosion resistance in elastomers is linked to their viscoelastic behaviour and low modulus prevents the pressure buildup, thus avoiding the stress concentrations across the surface, making them a better candidate for heavy rain impact erosions [44]. However, elastomers frequently fail underneath the surface under repetitive loads, while the surface remains intact. The erosion process on the fibre-reinforced elastomeric coatings could be explained by two modes. Firstly, the local resin removal may result in the exposure of fibres to the erosive environment. Secondly, there could be breakage of fibres as a result of direct impingement and cracks may start to form around and perpendicular to the fibre length as shown in figures 5c and 5d. Erosion impact on unfilled thermoset polymers induces breakage and massive chunking of resin due to their brittle behaviour. A massive increase in surface roughness was observed on the unfilled PU coatings in this study, as illustrated in figure 3b and supplementary figure 1a. Instead, the incorporation of fibres in the resins results in chipping and fracture of fibres instead of polymeric fractures, and the composite's ability to withstand repetitive impact loads is greatly enhanced. The degree of surface cracks can be greatly reduced on the coating surface after the incorporation of fibres. Fibres also hold the polymeric structure in place and provide a discontinuous path for shock transmission through the material as compared to the pure polymeric resin, as simulated in figure 7c.

To conclude, the fibre structures in elastomeric coatings effectively distribute the water droplets/sands energy across the composite structures without significant damage to the polyurethane matrix. The inclusion of fibres is also known to prevent crack initiations, making them the ideal candidate for icephobic applications, particularly since cracks serve as possible ice anchoring points. Specifically, carbon fibre reinforced coatings are promising candidates for icephobic applications as they have superior fatigue resistance as compared to Kevlar fibre filled composites [48]. Our experiments confirmed that the carbon fibre reinforced coatings had better erosion resistance and the surface cavities were much smaller on Kevlar fibre-reinforced coatings. Carbon fibre reinforced elastomeric coatings have all four characteristics for ideal durable icephobic coatings: higher erosion resistance, inhibition of surface cracks, ability to resist the plastic deformation, and stiff fibres to withstand against the significant structural loading conditions.

4 Conclusions

A new approach was developed to enhance the durability of low ice adhesion polyurethane coatings in this study. The incorporation of micro-fibres and nanoparticles in the coating matrix was driven by the need of enhancing durability in surface icephobicity under erosion impact. Ice adhesion strength after erosion was maintained to a low level with the incorporation of the fillers as compared to the pure PU coatings.

It was found that the fibre reinforcement was more effective in restricting the surface damage as compared to the addition of nanofillers. The ice adhesion strengths on the pristine and impinged PU coatings were 2.6 kPa and 83.1 kPa, respectively. As a comparison, the ice adhesion strength of the PU coatings with 20 wt% carbon fibres slightly increased from 5.6 kPa to 8.4 kPa, essentially keeping the adhesion below 10 kPa even after the erosion, and a ~10-fold reduction in ice adhesion strength was achieved as compared to that of the pure PU coatings. This distinction could be explained by better interfacial bonding and higher aspect ratio of the carbon fibres in the PU matrix.

The significantly improved icephobic durability of the carbon fibre-reinforced PU coatings could be attributed to the reduced number and shallowed surface cavities. The number/size of surface cavities formed during water erosion, which could act as possible ice anchoring points, were minimized with the incorporation of the fillers. The inclusion of fibres helps to distribute the droplet/sand impact energy more widely which could reduce the stress concentration in the coatings by minimizing crack initiation during the incubation period. The methodology proposed in this work can also be used for the durability enhancement of other polymeric coatings, especially the coatings designed for high-impingement conditions or erosive environments.

Acknowledgements

This work was supported by a studentship from the Faculty of Engineering, University of Nottingham and was partially funded by the CleanSky 2 Joint Undertaking under the European Union's Horizon 2020 research and innovation programme under grant agreement No CS2-AIR-GAM-2014-2015-O1. Cf. Art.29.4 of [A2]. The authors also thank Dr. Barbara Turnbull for helping with ice adhesion strength tests and acknowledge the use of facilities at the Nanoscale and Microscale Research Centre of the University of Nottingham supported by Engineering and Physical Sciences Research Council [grant number EP/L022494/1]. The authors are grateful to Teijin Aramid GmBH, Germany, for kindly supplying Twaron Kevlar fibres pulp.

References

[1] T. Mahmut, H. Memon, F. Xu, I. Ahmed, X. Hou, Electrospun nanofibre membrane based transparent slippery liquid-infused porous surfaces with icephobic properties, Colloids and Surfaces A: Physicochemical and Engineering Aspects 585 (2020) 124177.

[2] W. Cui, T.A. Pakkanen, Fabrication of transparent icephobic surfaces with self-reparability: Effect of structuring and thickness of the lubricant-elastomer layer, Applied Surface Science 504 (2020) 144061.

[3] K. Golovin, A. Dhyani, M. Thouless, A. Tuteja, Low–interfacial toughness materials for effective large-scale deicing, Science 364(6438) (2019) 371-375.

[4] J. Liu, J. Wang, H. Memon, Y. Fu, T. Barman, K.-S. Choi, X. Hou, Hydrophobic/icephobic coatings based on thermal sprayed metallic layers with subsequent surface functionalization, Surface and Coatings Technology 357 (2019) 267-272.

[5] E. Vazirinasab, K. Maghsoudi, R. Jafari, G. Momen, A comparative study of the icephobic and self-cleaning properties of Teflon materials having different surface morphologies, Journal of Materials Processing Technology 276 (2020) 116415.

[6] R.K. Moghadam, M.T. Rahni, K. Javadi, S.H. Davoudian, R. Miller, Influence of New Superhydrophobic Micro-structures on Delaying Ice Formation, Colloids and Surfaces A: Physicochemical and Engineering Aspects (2020) 124675.

[7] F. Piscitelli, A. Chiariello, D. Dabkowski, G. Corraro, F. Marra, L.D. Palma, Superhydrophobic Coatings as Anti-Icing Systems for Small Aircraft, Aerospace 7(1) (2020) 2.

[8] Y. Shen, Y. Wu, J. Tao, C. Zhu, H. Chen, Z. Wu, Y. Xie, Spraying fabrication of durable and transparent coatings for anti-icing application: dynamic water repellency, icing delay, and ice adhesion, ACS applied materials & interfaces 11(3) (2018) 3590-3598.

[9] Z.A. Janjua, B. Turnbull, K.-L. Choy, C. Pandis, J. Liu, X. Hou, K.-S. Choi, Performance and durability tests of smart icephobic coatings to reduce ice adhesion, Applied Surface Science 407 (2017) 555-564.

[10] J.H. Kim, M.J. Kim, B. Lee, J.M. Chun, V. Patil, Y.-S. Kim, Durable ice-lubricating surfaces based on polydimethylsiloxane embedded silicone oil infused silica aerogel, Applied Surface Science (2020) 145728.

[11] D. Wu, L. Ma, F. Zhang, H. Qian, B. Minhas, Y. Yang, X. Han, D. Zhang, Durable deicing lubricant-infused surface with photothermally switchable hydrophobic/slippery property, Materials & Design 185 (2020) 108236.

[12] J. Wang, H. Memon, J. Liu, G. Yang, F. Xu, T. Hussain, C. Scotchford, X. Hou, Effect of surface adsorption on icing behaviour of metallic coating, Surface and Coatings Technology 380 (2019) 125068.

[13] K. Golovin, S.P. Kobaku, D.H. Lee, E.T. DiLoreto, J.M. Mabry, A. Tuteja, Designing durable icephobic surfaces, Science advances 2(3) (2016) e1501496.

[14] W. Tong, D. Xiong, N. Wang, Z. Wu, H. Zhou, Mechanically robust superhydrophobic coating for aeronautical composite against ice accretion and ice adhesion, Composites Part B: Engineering 176 (2019) 107267.

[15] Y. Zhuo, S. Xiao, V. Håkonsen, T. Li, F. Wang, J. He, Z. Zhang, Ultrafast self-healing and highly transparent coating with mechanically durable icephobicity, Applied Materials Today 19 (2020) 100542.

[16] X. Wu, X. Zhao, J.W.C. Ho, Z. Chen, Design and durability study of environmental-friendly room-temperature processable icephobic coatings, Chemical Engineering Journal 355 (2019) 901-909.

[17] Y.H. Yeong, A. Milionis, E. Loth, J. Sokhey, Self-lubricating icephobic elastomer coating (SLIC) for ultralow ice adhesion with enhanced durability, Cold Regions Science and Technology 148 (2018) 29-37.

[18] F. Wang, W. Ding, J. He, Z. Zhang, Phase transition enabled durable anti-icing surfaces and its DIY design, Chemical Engineering Journal 360 (2019) 243-249.

[19] X. Wu, Z. Chen, A mechanically robust transparent coating for anti-icing and self-cleaning applications, Journal of Materials Chemistry A 6(33) (2018) 16043-16052.

[20] D.L. Beemer, W. Wang, A.K. Kota, Durable gels with ultra-low adhesion to ice, Journal of Materials Chemistry A 4(47) (2016) 18253-18258.

[21] Y. Zhuo, T. Li, F. Wang, V. Håkonsen, S. Xiao, J. He, Z. Zhang, An ultra-durable icephobic coating by a molecular pulley, Soft Matter 15(17) (2019) 3607-3611.

[22] J. Liu, J. Wang, L. Mazzola, H. Memon, T. Barman, B. Turnbull, G. Mingione, K.-S. Choi, X. Hou, Development and evaluation of poly (dimethylsiloxane) based composite coatings for icephobic applications, Surface and Coatings Technology 349 (2018) 980-985.

[23] H. Memon, J. Liu, N. Weston, J. Wang, D.S. De Focatiis, K.-s. Choi, X. Hou, In-situ icing and water condensation study on different topographical surfaces, Cold Regions Science and Technology 165 (2019) 102814.

[24] H. Memon, J. Liu, D.S. De Focatiis, K.-s. Choi, X. Hou, Intrinsic dependence of ice adhesion strength on surface roughness, Surface and Coatings Technology 385 (2020) 125382.

[25] S. Kulinich, M. Farzaneh, Ice adhesion on super-hydrophobic surfaces, Applied Surface Science 255(18) (2009) 8153-8157.

[26] C. Laforte, A. Beisswenger, Icephobic material centrifuge adhesion test, Proceedings of the 11th International Workshop on Atmospheric Icing of Structures, IWAIS, Montreal, QC, Canada, 2005, pp. 12-16.

[27] C. Laforte, C. Blackburn, J. Perron, and R. Aubert, Icephobic coating evaluation for aerospace application. In 55th AIAA/ASMe/ASCE/AHS/SC Structures, Structural Dynamics, and Materials Conference, 2014, pp. 1327.

[28] S. Rønneberg, Y. Zhuo, C. Laforte, J. He and Z. Zhang, Interlaboratory study of ice adhesion using different techniques, Coatings 9(10) (2019) 678.

[29] J.D. Pampush, D.J. Daegling, A.E. Vick, W.S. McGraw, R.M. Covey and A.J. Rapoff Technical note: Converting durometer data into elastic modulus in biological materials, Am. J. Phys. Anthropol 146 (2011) 650-653.

[30] I.M. Meththananda, S. Parker, M.P. Patel and M. Braden, The relationship between Shore hardness of elastomeric dental materials and Young's modulus, Dental materials, 25(8) (2009) 956-959.

[31] C. Wang, T. Fuller, W. Zhang, K.J. Wynne, Thickness dependence of ice removal stress for a polydimethylsiloxane nanocomposite: Sylgard 184, Langmuir 30(43) (2014) 12819-12826.

[32] I. Neitzel, V. Mochalin, I. Knoke, G.R. Palmese, Y. Gogotsi, Mechanical properties of epoxy composites with high contents of nanodiamond, Composites science and technology 71(5) (2011) 710-716.

[33] V.N. Mochalin, Y. Gogotsi, Nanodiamond–polymer composites, Diamond and Related Materials 58 (2015) 161-171.

[34] S. Roy, K. Mitra, C. Desai, R. Petrova, S. Mitra, Detonation nanodiamonds and carbon nanotubes as reinforcements in epoxy composites—a comparative study, Journal of Nanotechnology in Engineering and Medicine 4(1) (2013).

[35] D. Cai, K. Yusoh, M. Song, The mechanical properties and morphology of a graphite oxide nanoplatelet/polyurethane composite, Nanotechnology 20(8) (2009) 085712.

[36] B. Fiedler, F.H. Gojny, M.H.G. Wichmann, M.C.M. Nolte, K. Schulte, Fundamental aspects of nano-reinforced composites, Composites Science and Technology 66(16) (2006) 3115-3125.

[37] R.E. Lavengood, L.B. Gulbransen, The effect of aspect ratio on the fatigue life of short boron fiber reinforced composites, Polymer Engineering & Science 9(5) (1969) 365-369.

[38] O.G. Engel, Erosion damage to solids caused by high speed collision with rain, Journal of Research of the National Bureau of Standards 61(1) (1958) 47-52.

[39] O. Gohardani, Impact of erosion testing aspects on current and future flight conditions, Progress in Aerospace Sciences 47(4) (2011) 280-303.

[40] J.H. Brunton, F.P. Bowden, A discussion on deformation of solids by the impact of liquids, and its relation to rain damage in aircraft and missiles, to blade erosion in steam turbines, and to cavitation erosion - High speed liquid impact, Philosophical Transactions of

the Royal Society of London. Series A, Mathematical and Physical Sciences 260(1110) (1966) 79-85.

[41] D. Eisenberg, S. Laustsen, J. Stege, Wind turbine blade coating leading edge rain erosion model: Development and validation, Wind Energy 21(10) (2018) 942-951.

[42] H. Slot, E. Gelinck, C. Rentrop, E. Van Der Heide, Leading edge erosion of coated wind turbine blades: Review of coating life models, Renewable Energy 80 (2015) 837-848.

[43] B. Amirzadeh, A. Louhghalam, M. Raessi, M. Tootkaboni, A computational framework for the analysis of rain-induced erosion in wind turbine blades, part II: Drop impact-induced stresses and blade coating fatigue life, Journal of Wind Engineering and Industrial Aerodynamics 163 (2017) 44-54.

[44] M. Elhadi Ibrahim, M. Medraj, Water Droplet Erosion of Wind Turbine Blades: Mechanics, Testing, Modeling and Future Perspectives, Materials 13(1) (2020) 157.

[45] M. Mahdipoor, H. Kirols, D. Kevorkov, P. Jedrzejowski, M. Medraj, Influence of impact speed on water droplet erosion of TiAl compared with Ti6Al4V, Scientific reports 5 (2015) 14182.

[46] W. Adler, The mechanics of liquid impact, Academic Press, Treatise on Materials Science and Technology 16 (1979) 127-183.

[47] W. Adler, R. Vyhnal, Rain erosion of Ti-6Al-4V, Proceedings, AA Fyall and RB King, eds 2 (1974) 539-569.

[48] J.D. Buckley, D.D. Edie, Carbon-carbon materials and composites, William Andrew, 1993.

List of Figures

Supplementary information

Durability Enhancement of Low Ice Adhesion Polymeric Coatings

Halar Memon, Davide S.A. De Focatiis, Kwing-So Choi and Xianghui Hou*

Faculty of Engineering, University of Nottingham, University Park, Nottingham NG7 2RD, UK;

*Correspondence: xianghui.hou@nottingham.ac.uk.

Supplementary Table 1: Complete list of the results

Coating names	**Filler**	**Filler (wt %)**	**Before WIETs**						**After WIETs**		**Shore Hardness (Scale D)**
			WCA (°)	**AWCA (°)**	**RWCA (°)**	**CAH (°)**	**Ice adhesion strength (kPa)**	**R_a (µm)**	**Ice adhesion strength (kPa)**	**R_a (µm)**	
PU	-	-	66 ± 1	68 ± 1	44 ± 1	24 ± 2	2.6 ± 1	0.08 ± 0.01	83.1 ± 11	0.45 ± 0.05	40 ± 3
PU-CF-0.5	Carbon Fiber	0.5	64 ± 1	75 ± 1	41	34 ± 1	4.1 ± 1	0.07 ± 0.01	-	-	54 ± 3
PU-CF-1	Carbon Fiber	1	64 ± 2	72	43 ± 1	28 ± 2	5.3 ± 2	0.06 ± 0.01	-	-	54± 4
PU-CF-3	Carbon Fiber	3	59 ± 5	68 ± 1	41 ± 1	27 ± 2	5.6 ± 1	0.07 ± 0.01	16.8 ± 0.5	0.27 ± 0.03	55 ± 1
PU-CF-5	Carbon Fiber	5	63 ± 3	69 ± 1	41 ± 1	28 ± 1	6.7 ± 2	0.08 ± 0.01	-	-	55 ± 3
PU-CF-20	Carbon Fiber	20	60 ± 1	66 ± 3	39 ± 2	27 ± 3	5.8 ± 1	0.12 ± 0.03	8.4 ± 1	0.15 ± 0.02	65 ± 6
PU-KV-0.5	Kevlar Fiber	0.5	72 ± 4	75 ± 2	44 ± 2	32 ± 3	12.3 ± 1	0.15 ± 0.01	-	-	58 ± 2
PU-KV-1	Kevlar Fiber	1	64 ± 1	73 ± 1	45	28 ± 1	7 ± 0.5	0.08 ± 0.01	-	-	63 ± 1
PU-KV-3	Kevlar Fiber	3	64 ± 5	73 ± 2	44	29 ± 2	5.1 ± 0.5	0.10 ± 0.01	16.1 ± 6	0.25 ± 0.02	63 ± 2
PU-KV-5	Kevlar Fiber	5	63 ± 2	68	43 ± 1	25 ± 1	6.8 ± 0.5	0.10 ± 0.01	-	-	65 ± 4
PU-KV-20	Kevlar Fiber	20	62 ± 2	66 ± 2	40 ± 4	26 ± 3	16.2 ± 1	0.12 ± 0.01	31.8 ± 4	0.22 ± 0.03	78 ± 7
PU-ND-0.5	Nanodiamond	0.5	67 ± 1	71	45 ± 1	26 ± 1	5.6 ± 0.5	0.11 ± 0.01	-	-	47 ± 1
PU-ND-1	Nanodiamond	1	65 ± 4	70 ± 1	43 ± 1	26 ± 2	3.9 ± 0.5	0.06 ± 0.01	-	-	49 ± 3
PU-ND-3	Nanodiamond	3	62 ± 1	68 ± 1	46	22 ± 1	2.7 ± 0.5	0.07 ± 0.01	45.4 ± 8	0.21 ± 0.04	55 ± 2
PU-ND-5	Nanodiamond	5	61 ± 3	67 ± 1	45 ± 1	22	2.7 ± 0.5	0.04 ± 0.01	-	-	57 ± 5
PU-ND-20	Nanodiamond	20	60 ± 1	63 ± 1	37 ± 1	26 ± 2	3 ± 0.5	0.07 ± 0.01	39.9 ± 5	0.24 ± 0.03	72 ± 8
PU-ND-40	Nanodiamond	40	54 ± 1	61 ± 1	26	35 ± 1	4.8 ± 0.5	0.11 ± 0.01	28.9 ± 7	0.17 ± 0.02	74 ± 6
PU-GR-0.5	Graphene	0.5	67 ± 5	65 ± 2	37 ± 1	28 ± 1	4 ± 0.5	0.07 ± 0.01	-	-	45 ± 1
PU-GR-1	Graphene	1	60 ± 3	64 ± 2	38	26 ± 2	3.8 ± 0.5	0.06 ± 0.01	-	-	47 ± 1
PU-GR-3	Graphene	3	60 ± 5	70 ± 1	43 ± 1	27 ± 2	2.8 ± 0.5	0.10 ± 0.01	43.3 ± 6	0.21 ± 0.03	47 ± 3
PU-GR-5	Graphene	5	69 ± 3	76 ± 1	44 ± 3	32 ± 3	11.7 ± 2	0.12 ± 0.01	-	-	48 ± 2

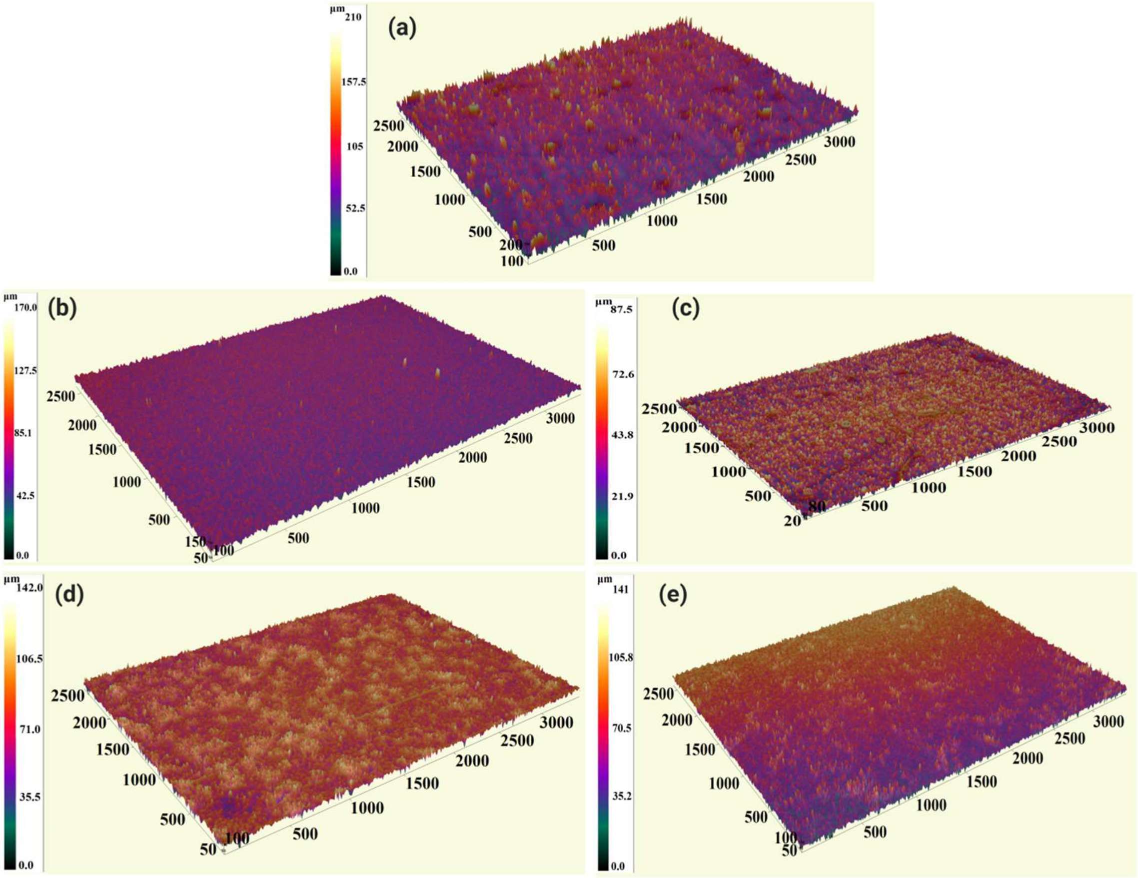

Sup. Fig. 1: 3D surface profile of (a) pure PU, (b) PU-ND-3, (c) PU-GR-3, (d) PU-KV-3, and (e) PU-CF-3 coatings after WIETs.

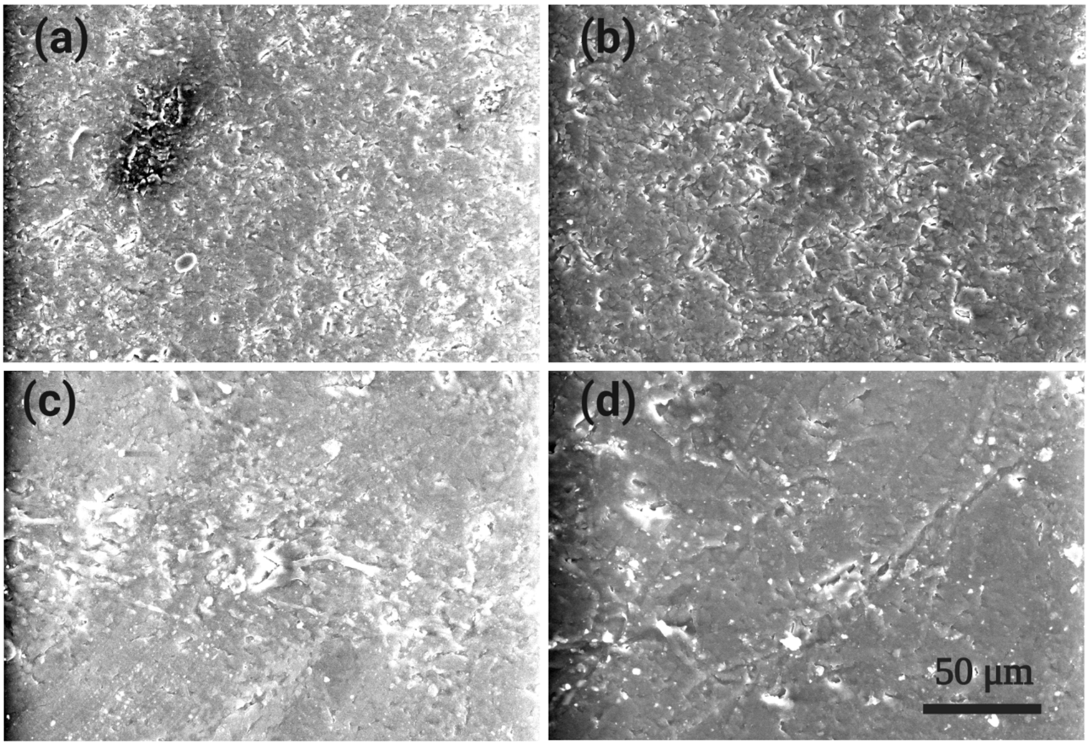

Sup. Fig. 2: Microstructural images of (a) PU-GR-3, (b) PU-ND-3, (c) PU-CF-3, and (d) PU-KV-3 coatings after WIETs. All images have the same scale bar.

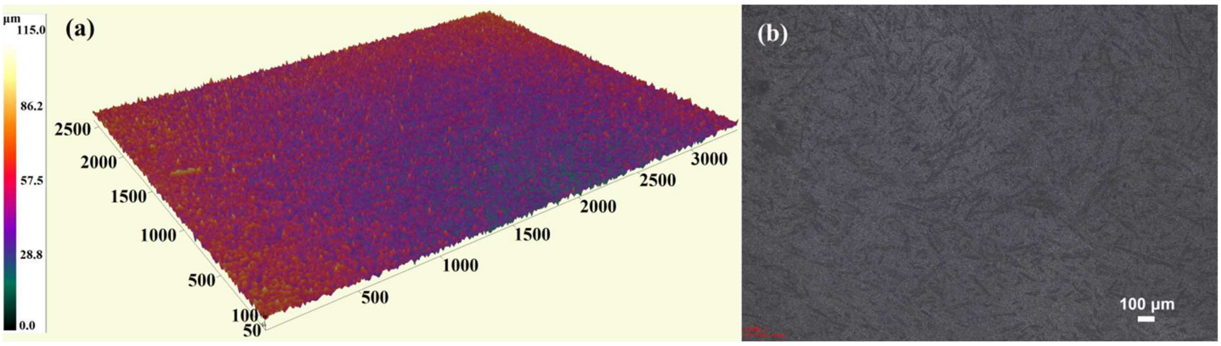

Sup. Fig. 3: (a) 3D profile and (b) 2D image of PU-CF-20 coatings after WIETs.